frontiers in Physics

ORIGINAL RESEARCH
published: 07 June 2021
doi: 10.3389/fphy.2021.697719

Construction of Optical Topological Cavities Using Photonic Crystals

Meng Yuan[1], *Tao Xu*[1,2] *and Zhi Hong Hang*[1,3]*

[1]School of Physical Science and Technology and Collaborative Innovation Center of Suzhou Nano Science and Technology, Soochow University, Suzhou, China, [2]Shenzhen Kuang-Chi Institute of Advanced Technology, Shenzhen, China, [3]Institute for Advanced Study, Soochow University, Suzhou, China

A novel design of the Fabry–Pérot optical cavity is proposed, utilizing both the topological interface state structures and photonic bandgap materials with a controllable reflection phase. A one-to-one correspondence between the traditional Fabry–Pérot cavity and optical topological cavity is found, while the tunable reflection phase of the photonic crystal mirrors provides an extra degree of freedom on cavity mode selection. The relationship between the Zak phase and photonic bandgap provides theoretical guidance to the manipulation of the reflection phase of photonic crystals. The dispersions of interface states with different topology origins are explored. Linear interfacial dispersion emerging in photonic crystals with the valley–spin Hall effect leads to an extra $n = 0$ cavity mode compared to the Zak phase–induced deterministic interface states with quadratic dispersion. The frequency of the $n = 0$ cavity mode is not affected by the cavity length, whose quality factor can also be tuned by the thickness of the photonic crystal mirrors. With the recent help of topology photonics in the tuning reflection phase and dispersion relationship, we hope our results can provide more intriguing ideas to construct topological optical devices.

Keywords: photonic crystal, topological interface states, reflection phase, Zak phase, valley–spin Hall effect

OPEN ACCESS

Edited by:
Guancong Ma,
Hong Kong Baptist University, China

Reviewed by:
Xueqin Huang,
South China University of Technology, China
Meng Xiao,
Hong Kong University of Science and Technology, China

***Correspondence:**
Zhi Hong Hang
zhhang@suda.edu.cn

Specialty section:
This article was submitted to Optics and Photonics, a section of the journal Frontiers in Physics

Received: *20 April 2021*
Accepted: *17 May 2021*
Published: *07 June 2021*

Citation:
Yuan M, Xu T and Hang ZH (2021) Construction of Optical Topological Cavities Using Photonic Crystals. Front. Phys. 9:697719. doi: 10.3389/fphy.2021.697719

INTRODUCTION

In 2008, Haldane and Raghu [1, 2] introduced topology to photonics, opening a brand-new research direction in the realm of photonics: topological photonics [3, 4]. Various topological invariants, having been applied to topological insulators, can also be used to characterize the properties of photonic bulk bands. When two optical materials, characterized by different topological properties, are placed in proximity, robust edge states emerge along their interfaces which could accommodate backscattering-immune electromagnetic propagations. After the first demonstration of a unidirectional optical waveguide [5], the Chern number, as the quantized flux of the Berry curvature through the whole Brillouin zone (BZ), has triggered various designs in electronic [6], photonic [7–9], and cold atom [10] systems. The Zak phase [11], a one-dimensional (1D) geometric phase, was also found to be capable of describing bulk photonic band properties [12]. It was further extended to two-dimensional (2D) and deterministic waveguiding in both acoustic and photonic systems [13–16]. Different from the systems characterized by the Chern number, that time reversal symmetry is broken; the inverted symmetry breaking results in a sign opposite to that of the Berry curvature near the two inequivalent BZ corners where the valley Chern number [17–19] can be defined and unidirectional valley pseudospin propagation was observed [20–23]. With the help of these topologically induced unidirectional electromagnetic propagations, various novel designs, such as optical delay lines [24], valley couplers [25], and nonlinear optical devices [26], have been

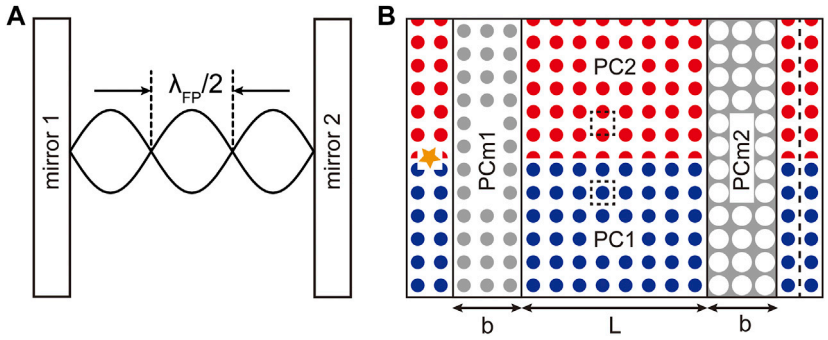

FIGURE 1 | (A) Sketch of a traditional FP cavity. Light of wavelength λ_{FP} will exist in such a cavity. **(B)** The schematic diagram of OTC type **I** constructed by 2D PCs. PC1 and PC2 are with different Zak phases where interface states are induced along their interface within the common photonic bandgap of PCm1 and PCm2 (in gray). Two PC mirrors are considered to replace the original reflecting mirrors.

successfully demonstrated. Moreover, major research attention has also been devoted to laser operations, employing the topological interface states [27–33]. Different topological interface state designs, based on mechanisms such as the Su–Schrieffer–Heeger (SSH) model [27, 28], magneto-optical effect [29], coupled ring–resonator array [30], spin Hall effect [31], and valley–spin Hall effect [32], have been applied to increase the total emission power in topological cavities and maintain a stable single-mode emission of the whole system. Topological bulk lasing is also possible by engineering band-inversion–induced reflection [33].

In a traditional laser, the Fabry–Pérot (FP) cavity, in which photons bounce back and forth in the lasing medium between two parallel plane mirrors (as shown in **Figure 1A**), is an important component to provide light energy feedback. Furthermore, it also plays an important role in frequency selection. In this article, we extend the study of topological photonics to the design of the FP laser cavity by using 2D topological photonic crystals (PCs). Different from previous studies where only topologically induced interface modes were employed, we also design the reflection mirrors of PCs based on topological photonics. By assembling different PCs with topologically induced interface states and different PC mirrors with different reflection properties, we can construct optical topological cavities (OTCs) with tunable properties. Two different types of OTCs, based on different topological interface states, are designed and compared with the physics discussed below. The PC-based reflection mirrors also provide a degree of freedom for mode selection, and an efficient approach to tune the cavity fidelity is also discussed.

DESIGNS AND RESULTS

Optical Topological Cavity Type I

As shown in **Figure 1A**, a traditional FP cavity is composed of parallel cavity mirrors and a lasing medium in between. The laser wavelength λ_{FP} to be selected depends on the distance between the two cavity mirrors: $n\lambda_{FP}/2 = L_{cavity}$, where L_{cavity} is the distance between the two mirrors and n indicates its index. Our construction principle for OTCs is to use topologically induced interface states to replace the lasing medium and PC mirrors to replace the cavity mirrors. A scheme of OTC type I is depicted in **Figure 1B**. In OTC type I, the Zak phase–induced interface states are employed where PC2 is the counterpart of the cylinder-arrayed PC1 with a shifted lattice [15]. The cavity length L is defined as the number of columns of PCs used. Photonic bandgap materials will serve as reflecting mirrors, and as an example, mutually inverted 2D PCs with thickness b are used as illustrated in gray. Other PC mirrors can also be considered. In this work, we carry out numerical simulations using the finite element method [34] to study the properties of such OTCs. A point source (denoted as an orange star in **Figure 1B**) is used to excite the cavity modes, and its transmission spectrum is obtained by a line integral along the black dotted line on the right side of the cavity. Within the gap frequencies of PC mirrors, the peaks existing in the transmission spectrum denote the cavity modes excited.

Here, we consider the transverse magnetic (TM, with electric field E_Z along cylinder axis) polarization. The calculated photonic band diagrams of the PC1 and PC2 are shown in **Figure 2A**. PC2 (in red) is identical to PC1 (in blue) of a square array of dielectric cylinders except that its unit cell is shifted by half a lattice constant a along the y direction. The radius of cylinders for PC1 and PC2 is $r_1 = 0.282a$. In **Figure 1B**, colored regions (red, blue, and gray) indicate where dielectric materials with $\varepsilon_{diel} = 10.5$ are used and air is assumed in other regions. With identical unit cells, PC1 and PC2 possess the same band diagram with a common bandgap above the first photonic band. It is discussed and experimentally verified [15, 16] that the Zak phase of the first band is inverted between PC1 and PC2; thus, an interface state would emerge if PC1 and PC2 are assembled, as shown in the black line in **Figure 2B**. Here, we consider a supercell with 15 unit cells of both PCs, and periodic boundaries are applied along both the x and y directions. Electromagnetic waves will propagate along the interface within the frequency range between 0.2521 and $0.3021c/a$. The major physical reason that the interface state shall arouse along the interface is that the reflection phase $\varphi_{PC1(2)}$ on PC1(2) is of a different sign, and when $\varphi_{PC1} + \varphi_{PC2} = 0$, an interface state emerges [15]. The reflection phase of PCs plays a

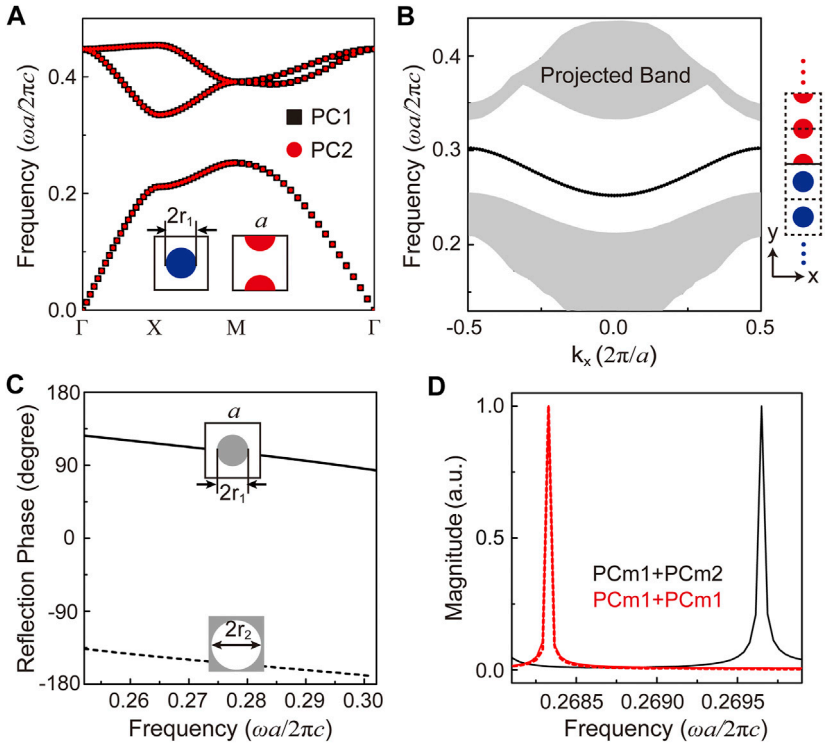

FIGURE 2 | (A) TM photonic band diagrams of PC1 and PC2 with shifted lattice. **(B)** Calculated projected band structure with a supercell of PC1 and PC2 assembled along the *y* direction. The folded bulk bands of PC1 and PC2 are painted in gray, and the interface state is in black. **(C)** The reflection phases upon PC mirrors. **(D)** By changing PC mirrors, the cavity mode frequency will change. Red lines indicate the scenario where PCm1 serves as both cavity mirrors, and the black line indicates the scenario where PCm1 and PCm2 serve as the two cavity mirrors, respectively. A slab of effective parameters ε = −2.8 and μ = 1.2 with a reflection phase 113.578°is also considered to replace PCm1, whose reflection phase is the same as that of PCm1 at 0.2683 *c/a*.

key role in the emergence of such an interface state. Will the reflection phase play a role similar to that of the PC mirrors? PCm1 is chosen to be the same as PC1, and its reflection phase is calculated to be between 83.551 and 126.542°, within the frequency range of the interface state dispersion. If we consider a similar cylinder-in-air geometry and at the first photonic bandgap, we shall obtain a reflection phase with similar values. On the contrary, as discussed in Huang et al. [14], an inverted PC, with air holes in a dielectric slab, will have inverted the Zak phase as well as the reflection phase at the photonic gap above the first band. In other words, the reflection on an inverted PCm2 constructed by drilling air holes of radius $r_2 = 0.473a$ in the dielectric slab will be totally different from that with cylinder-in-air geometry, where its calculated reflection phase is found between −170.309 and −136.291°, as shown in **Figure 2C**. OTC type I is thus constructed with the Zak phase–induced interface as the lasing medium and PCs with inverted structures as mirrors, as depicted in **Figure 1B**. In **Figure 2D**, the calculated transmission spectrum of OTC type I is plotted with the cavity length $L = 11a$ and mirror thickness $b = 3a$. A cavity mode, peaked at 0.2696 *c/a*, is excited. What if PC mirrors are changed? By replacing PCm2 back to PCm1, an obvious shift of the cavity mode is acquired.

In the studies of traditional FP cavities, the reflection phase of mirrors has never been considered. The major reason is that in a traditional FP cavity, metallic mirrors are considered with a 180° reflection phase. During the back-and-forth bouncing between these two mirrors, no phase accumulation will occur. On the contrary, although total reflection occurs on PCm1/PCm2, the frequency shift we observe shall correspond to their different reflection phases. Electromagnetic waves propagate along the interface and then bounce back on one PC mirror with the accumulated phase and propagate again along the interface. Thus, the FP condition of a cavity shall be revised as

$$\varphi_{\mathrm{PCm1}} + \varphi_{\mathrm{PCm2}} + 2k(\omega)L = 2n\pi, \tag{1}$$

where $\varphi_{\mathrm{PCm1\,(2)}}$ is the reflection phase on PCm1(2) in the radian unit, $k(\omega)$ is the wave number (in the unit of $2\pi/2$) of the interface state at different frequency ω, L is the length of the OTC, and n is an integer. **Eq. 1** can be easily reduced to the FP condition if inserting $\varphi_{\mathrm{PCm1}} = \varphi_{\mathrm{PCm2}} = \pi$ and $k(\omega) = 2\pi/\lambda_{\mathrm{FP}}$. From **Eq. 1**, we can easily see that using PC mirrors will provide an effective approach to tune the reflection phases and the mode to be selected. However, the precise verification of **Eq. 1** is not straightforward as both the reflection phases of PCs and the dispersion of the interface states are frequency dependent. As total reflection occurs here for PC mirrors, a simpler approach is to replace PC mirrors with effective medium slabs with a single negative value of permittivity/permeability, where the arbitrary

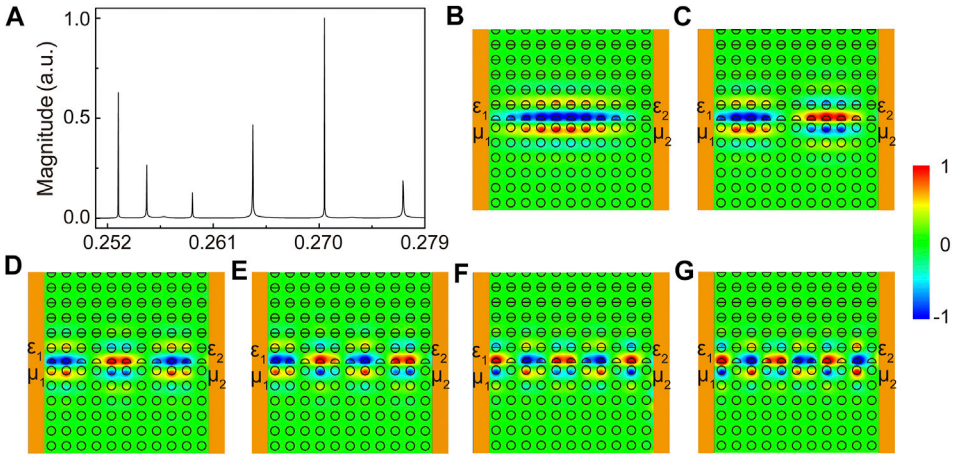

FIGURE 3 | (A) The calculated transmission spectrum with PC mirrors replaced by single negative effective medium slabs. **(B–G)** Simulated E_Z field distributions at 0.2529, 0.2553, 0.2592, 0.2644, 0.2705, and 0.2771 *c*/*a*.

TABLE 1 | Cavity modes at length $L = 11a$.

n	f(c/a)	k(π/a)	k$'$ (π/a)	2 *kl*
1	0.2529	0.090	0.091	1.988π
2	0.2553	0.182	0.182	4.000π
3	0.2592	0.273	0.272	5.999π
4	0.2644	0.363	0.364	7.997π
5	0.2705	0.454	0.455	9.986π
6	0.2771	0.544	0.545	11.968π

reflection phase can be tuned. As shown in the dashed line in **Figure 2D**, by replacing PCm1 with a slab with $\varepsilon = -2.8$, $\mu = 1.2a$, whose reflection phase is the same as that of PCm1 at the frequency 0.2683 *c*/*a*, a nearly identical spectrum is obtained, indicating the validity of our effective slab model. We thus can verify **Eq. 1** through numerical simulations by various slabs with tunable reflection phases. We change PCm1 to slab1 with $\varepsilon_1 = -3$, $\mu_1 = 2$ and PCm2 to slab2 with $\varepsilon_2 = 3$, $\mu_2 = -2$, and their reflection phase sum is $\varphi_{m1} + \varphi_{m2} = 0$. The slab thickness is *a*. As can be found in **Figure 3A**, multiple cavity modes are excited in OTC type I with $L = 11a$. The corresponding mode profiles (normalized to its own maximal intensity) can be found in **Figures 3B–G** at the frequencies 0.2529, 0.2553, 0.2592, 0.2644, 0.2705, and 0.2771 *c*/*a*, respectively. Red (blue) color indicates that the electric field is of positive (negative) value, which bears great similarity to the first of the sixth-order FP modes. It is the fifth-order FP mode that we achieved, as shown in **Figure 2D**.

Further analysis is conducted as shown in **Table 1**. We can find its corresponding wave number *k* at the transmission spectrum peak frequency in our calculated dispersion, as shown in **Figure 2B**. Thus, the total phase accumulation 2 *kl* with $\varphi_{m1} + \varphi_{m2} = 0$ is very close to the corresponding *n* multiplied by 2π. For comparison, we can also obtain the corresponding wave number k' by the fast Fourier transformation of the corresponding electric field distribution as shown in **Figures 3B–G**, where good consistency can be found with our dispersion readout.

Optical Topological Cavity Type II

Using Zak phase–induced interfaces, we have successfully constructed OTC type I and discovered the role PC mirrors play in the mode selection. As various applications have been demonstrated utilizing the unidirectional interface states induced by the valley-spin Hall effect, we extend our work to construct OTC type II by using valley-spin Hall PCs. By introducing sublattice symmetry breaking into the honeycomb lattice PC [25], unidirectional interface states are induced and adopted to construct OTC type II. We consider PC3 and PC4 with inverted inversion symmetry. Here, three honeycomb lattices are considered as an enlarged hexagonal unit cell, with six dielectric cylinders with permittivity $\varepsilon'_{diel} = 7.5$ inside, as depicted in the inset of **Figure 4A**. If all six cylinders are of the same radius, with such an enlarged unit cell, the Dirac cones originally at BZ boundaries (K and K' points) of the honeycomb lattice will be folded to the BZ center (Γ point) to form a doubly degenerate Dirac cone. If neighboring cylinders are of different radii ($r_3 = 0.176a'$ and $r_4 = 0.147a'$, where a' is the side length of the hexagon unit cell), a bandgap opens in the calculated TM photonic band diagrams of PC3 and PC4, as shown in **Figure 4A**. PC3 and PC4 are of an identical unit cell but cylinders of radius r_3 are swapped with those of r_4. Assembling PC3 and PC4 along the lattice armchair orientation will give rise to unidirectional interface states, with the calculated interface dispersions (in green and orange) shown in **Figure 4B**. Here, we consider a supercell (shown in the right panel) consisting of five unit cells for both PC3 and PC4, with periodic boundary conditions applied along the *x* direction and scattering boundary conditions applied along the *y* direction. Interface states corresponding to valley pseudospins up (in green) intercross those of pseudospin down (in orange) linearly at Γ point, which is very different from the Zak phase–induced interface state, as shown in **Figure 2B**. A major difference between OTC type I and type II is that the

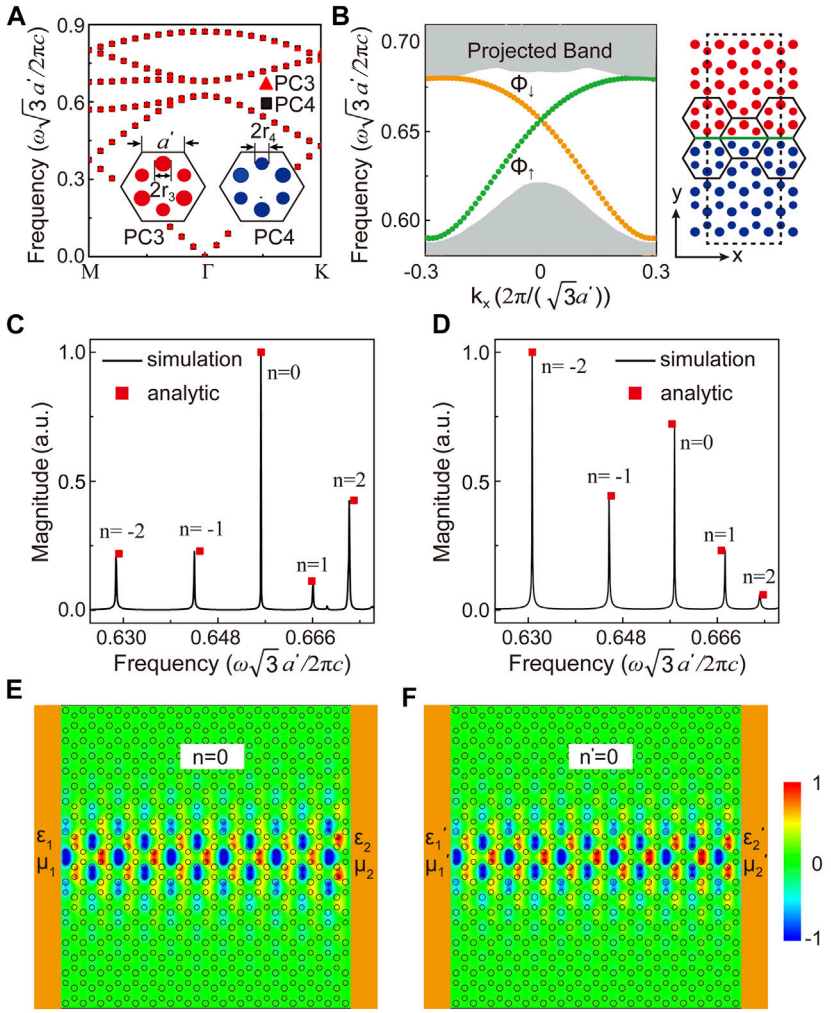

FIGURE 4 | (A) Calculated bulk TM photonic band diagrams of PC3 and PC4. As the diameters of cylinders in a unit cell are not identical in both PC3 and PC4 ($r_3 = 0.176a'$, $r_4 = 0.147a'$, and $\varepsilon'_{diel} = 7.5$), a photonic bandgap appears by sublattice symmetry breaking. **(B)** The projected band structure consists of five unit cells for both PC3 and PC4 along the *y* direction, shown in the right panel. The folded bulk bands belonging to PC3 or PC4 are painted in gray, whereas the two topological interface bands are shown by yellow dots. **(C,D)** The received transmission spectra for different effective medium slabs ($\varepsilon_1 = -5$, $\mu_1 = 1$; $\varepsilon_2 = 5$, $\mu_2 = -1$ and $\varepsilon'_1 = -6$, $\mu'_1 = 1$; $\varepsilon'_2 = 1.5$, $\mu'_2 = -1$) serving as two cavity mirrors, respectively. **(E,F)** Simulated E_Z field distributions of $n = 0$ and $n' = 0$ modes at 0.6562 and 0.6579 *c/a* (normalized to its own maximal intensity).

interface states are with linear or quadratic dispersion, which leads to their different performance, as we shall elaborate later.

We have shown in the previous section that using an effective medium slab can explain the role of PC mirrors in constructing an OTC, and thus, a pair of effective medium mirrors with zero total-reflecting phases is first considered here to construct OTC type II with $\varepsilon_1 = -5$, $\mu_1 = 1$ and $\varepsilon_2 = 5$, $\mu_2 = -1$. In **Figure 4C**, we show the calculated transmission spectrum through this OTC, where multiple peaks, inferring multiple cavity modes, are obtained. For comparison, as shown in **Figure 4D**, the spectrum of another set of slab mirrors, with $\varepsilon'_1 = -6$, $\mu'_1 = 1$ and $\varepsilon'_2 = 1.5$, $\mu'_2 = -1$ is considered with $\varphi_{m1} + \varphi_{m2} = 0.189\pi$, where all modes shift to higher frequency. But a detailed analysis from **Eq. 1** reveals some new physics. Instead of all-positive mode indices found in OTC type I, negative indices are also possible in OTC type II, as derived from **Eq. 1**. The field profiles of mode ± 1 (± 2) are very similar to each other and bear similarity to **Figures 3B and C**. Here, the corresponding analytical mode index is achieved by finding wave number *k* from **Eq. 1** and its readout of the frequency from the valley pseudospin up dispersion. Moreover, an extra $n = 0$ mode emerges. As can be seen in **Figure 4E**, the mode is almost homogenous along the whole interfacial region except for some variations in one unit cell, inferring no phase accumulation for electromagnetic waves during interfacial propagation.

The unidirectional property of valley–spin Hall interface states provides a totally different picture of the electromagnetic wave propagation inside OTC type II. As our source is on the left side of the OTC, only the valley pseudospin up state (the green-colored

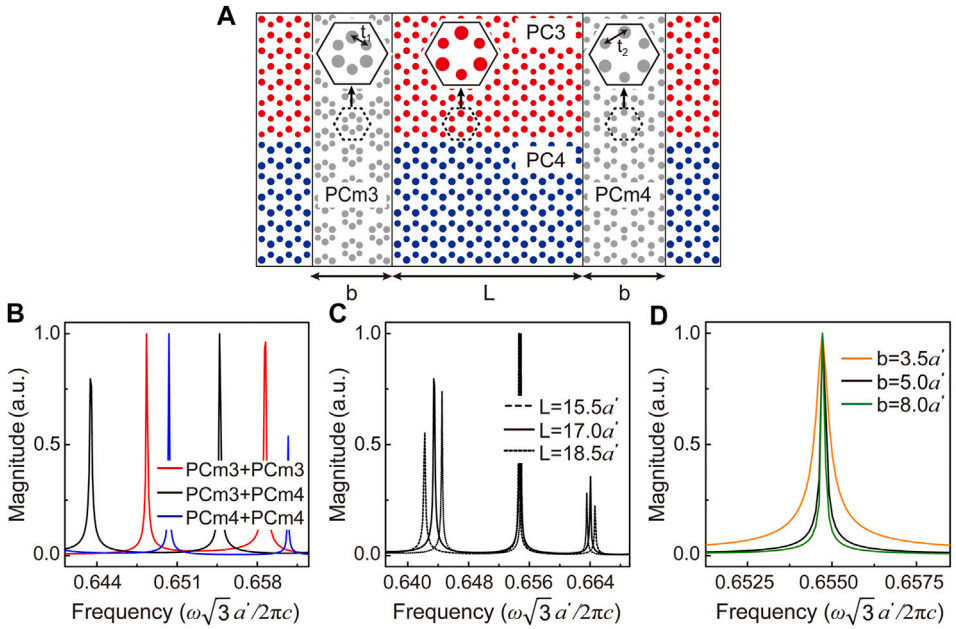

FIGURE 5 | (A) Schematics of OTC type II and 2 PC cavity mirrors. PCm3 (PCm4) is considered with a shrunken (expanded) lattice compared to the PC structure considered at the interface region. **(B)** The mode selection of different PC mirror configurations. **(C)** The received transmission spectra with different cavity lengths. **(D)** By tuning the thickness of PC mirrors, the cavity fidelity will be enhanced (b = 3.5a', Q = 1333.20; b = 5a', Q = 3418.46; and b = 8a', Q = 4830.43).

dispersion in **Figure 4B**) is excited to propagate rightward, whose wave number is decided by the corresponding frequency. With its linear dispersion, both positive and negative values of the wave number are possible and correspond to different frequencies. When bounced on the right mirror, the pseudospin up state must be flipped to the pseudospin down state as for the unidirectional property and a change of dispersion occurs. However, although the sign of the wave number changes accordingly, as for leftward propagation, further phase accumulation will occur to satisfy the FP condition as shown in **Eq. 1**. The phenomenon will be identical if the source is put on the right side of the OTC with an identical transmission spectrum to be received on the left side of the OTC. However, if the leftward propagation valley pseudospin down state is considered first, which is the case with source on the right, mode index n will be reversed such that the sequence of the peaks shall read as 2, 1, 0, −1, and −2, as in **Figures 4C and D**, respectively. This is quite different from OTC type I with a Zak phase–induced interface state with only positive indices. With its quadratic dispersion, the frequency with wave number k is the same as that of $-k$ and thus positive and negative indices are degenerate to each other.

The absence of n = 0 mode in OTC type I can also be understood from their dispersion difference. Although k = 0 (at Γ point) is possible for the Zak phase–induced interface state, time reversal symmetry requires that its dispersion be quadratic, whose group velocity is zero there. This slow light will not be physical and will not appear in our calculated spectrum. On the contrary, the finite group velocity of the linear dispersion of the valley–spin Hall effect at Γ point allows its emergence.

Knowing the physics of OTC type II, we can construct it using PC structures. We consider PC mirrors with deformed honeycomb lattice, where the positions of the six cylinders in PC3 and PC4 are changed. When the six cylinders in one unit cell are moved closer to the center of the unit cell, decreasing the intercylinder distance, a shrunken-latticed PCm3 is constructed where its expanded counterpart is considered as PCm4, both shown in gray in **Figure 5A**. The lattice deformation not only provides an extra mechanism for the bandgap opening of the linear dispersion of two interface states [35], but also leads to the quantum spin Hall effect of photonic crystals [36, 37]. With the bandgap of the interfacial state dispersion, PCm3 and PCm4 can serve as the PC mirrors for OTC type II. Of course, other honeycomb structures can be introduced as PC mirrors whose photonic bandgap frequency overlaps with the linear interfacial dispersion of the valley–spin Hall effect in the PC we design. The introduction of lattice deformation is the easiest approach (though not of the easiest geometry) to guarantee the bandgap with matched lattice. With the same dielectric material considered, this 2D design can be further extended to photonic slab geometry. The intercylinder distance is t_1 = 0.594a' for PCm3 and t_2 = 0.645a' for PCm4, and thus, they are with a common bandgap but different bulk topological properties. We thus can obtain the transmission spectra through OTC type II as illustrated in **Figure 5A**, and the results are shown in **Figures 5B–D**. By considering different PC mirror configurations, the obvious frequency shift of cavity modes can be achieved. The frequency shift is a consequence of the reflection phase difference between PCm3 and PCm4. It is totally understandable because of the different topological bulk

properties (Z_2 topological invariant) for expanded and shrunken lattices. In both OTC type I and type II, the use of PC mirrors with different reflection phases is an efficient approach to select the mode to be excited. From **Eq. 1** and the traditional FP cavity, the cavity mode will also be dependent on the cavity length L, except for the $n = 0$ mode, which only exists in OTC type II. As can be seen in **Figure 5C**, the frequency of the $n = 0$ mode remains at the frequency of 0.6548 c/a with different cavity lengths considered, but the frequency difference between other peaks becomes smaller for a longer cavity. Here, PCm3 and PCm4 are considered as cavity mirrors on either side. Mode fidelity is also a key property of optical cavities. The quality (Q) factor, the full-width half maximum of the $n = 0$ mode can be largely enhanced if the PC mirror thickness is increased. Although the results are obtained with cavity length $L = 17a^{'}$, as the frequency of the $n = 0$ mode is not sensitive to cavity length, the tuning of quality factor can be applied to other cavity designs.

DISCUSSION AND CONCLUSION

In summary, we extend the study of topology photonics to the construction of OTCs. Different topological invariants have been utilized for the generation of robust topological interface states with various applications triggered. Following the theoretical derivation based on the Zak phase and valley–spin Hall effect of light, respectively, different topologically induced interface states are designed and introduced in the construction of OTC type I (PCs with shifted lattice) and OTC type II (honeycomb lattice with broken inversion symmetry). Although one-to-one correspondence between a traditional FP optical planar mirror cavity and OTCs can be found, the quadratic interface dispersion in OTC type I and the linear interface dispersion in OTC type II govern the totally different mode selection criteria in the two OTCs. Negative and zeroth mode indices appear for OTC type II, solely because of its linear dispersion with topological origin. The zeroth mode maintains a constant working frequency irrespective of the length of the cavity.

We also extend the study of topological invariants to the design of the reflection phase in an OTC. We find that the reflection phase of PC mirrors adopted in the construction of OTC plays a key role in mode selection and will be essential when designing an OTC working at one particular frequency. The change of the topological invariant indicates a topology phase transition which also accompanies a dramatic reflection phase change at the associated photonic bandgap, which is verified for PC mirrors based on the Zak phase and quantum spin Hall effect. This new design principle to tune the reflection phase of PCs will help the future development of optical devices.

DATA AVAILABILITY STATEMENT

The original contributions presented in the study are included in the article/Supplementary Material, and further inquiries can be directed to the corresponding author.

AUTHOR CONTRIBUTIONS

ZH conceived the idea and wrote part of the manuscript. MY performed the numerical simulations and wrote part of the manuscript. MY and TX analyzed the results and prepared the figures. All authors have given approval to the final version of the manuscript.

FUNDING

This work is supported by the National Natural Science Foundation of China (Grant No. 11874274) and a project funded by the Priority Academic Program Development of Jiangsu Higher Education Institutions (PAPD). The authors are also grateful for the support from Jiangsu Key Laboratory of Thin Films and Jiangsu Key Lab of Advanced Optical Manufacturing Technologies.

ACKNOWLEDGMENTS

The authors would like to acknowledge Hua Jiang for his kind suggestions.

REFERENCES

1. Haldane FDM, and Raghu S. Possible Realization of Directional Optical Waveguides in Photonic Crystals with Broken Time-Reversal Symmetry. *Phys Rev Lett* (2008) 100:013904. doi:10.1103/PhysRevLett.100.013904
2. Raghu S, and Haldane FDM. Analogs of Quantum-Hall-Effect Edge States in Photonic Crystals. *Phys Rev A* (2008) 78:033834. doi:10.1103/PhysRevA.78.033834
3. Khanikaev AB, and Shvets G. Two-dimensional Topological Photonics. *Nat Photon* (2017) 11:763–73. doi:10.1038/s41566-017-0048-5
4. Ozawa T, Price HM, Amo A, Goldman N, Hafezi M, Lu L, et al. Topological Photonics. *Rev Mod Phys* (2019) 91:015006. doi:10.1103/RevModPhys.91.015006
5. Wang Z, Chong Y, Joannopoulos JD, and Soljačić M. Observation of Unidirectional Backscattering-Immune Topological Electromagnetic States. *Nature* (2009) 461:772–5. doi:10.1038/nature08293
6. Sheng DN, Weng ZY, Sheng L, and Haldane FDM. Quantum Spin-Hall Effect and Topologically Invariant Chern Numbers. *Phys Rev Lett* (2006) 97:036808. doi:10.1103/PhysRevLett.97.036808
7. Poo Y, Wu R, Lin Z, Yang Y, and Chan CT. Experimental Realization of Self-Guiding Unidirectional Electromagnetic Edge States. *Phys Rev Lett* (2011) 106:093903. doi:10.1103/PhysRevLett.106.093903
8. Skirlo SA, Lu L, and Soljačić M. Multimode One-Way Waveguides of Large Chern Numbers. *Phys Rev Lett* (2014) 113:113904. doi:10.1103/PhysRevLett.113.113904
9. Skirlo SA, Lu L, Igarashi Y, Yan Q, Joannopoulos J, and Soljačić M. Experimental Observation of Large Chern Numbers in Photonic Crystals. *Phys Rev Lett* (2015) 115:253901. doi:10.1103/PhysRevLett.115.253901
10. Price HM, Zilberberg O, Ozawa T, Carusotto I, and Goldman N. Measurement of Chern Numbers through Center-of-Mass Responses. *Phys Rev B* (2016) 93:245113. doi:10.1103/PhysRevB.93.245113
11. Zak J. Berry's Phase for Energy Bands in Solids. *Phys Rev Lett* (1989) 62:2747–50. doi:10.1103/PhysRevLett.62.2747

12. Xiao M, Ma G, Yang Z, Sheng P, Zhang ZQ, and Chan CT. Geometric Phase and Band Inversion in Periodic Acoustic Systems. *Nat Phys* (2015) 11:240–4. doi:10.1038/NPHYS3228
13. Yang Y, Huang X, and Hang ZH. Experimental Characterization of the Deterministic Interface States in Two-Dimensional Photonic Crystals. *Phys Rev Appl* (2016) 5:034009. doi:10.1103/PhysRevApplied.5.034009
14. Huang X, Yang Y, Hang ZH, Zhang ZQ, and Chan CT. Geometric Phase Induced Interface States in Mutually Inverted Two-Dimensional Photonic Crystals. *Phys Rev B* (2016) 93:085415. doi:10.1103/PhysRevB.93.085415
15. Yang Y, Xu T, Xu YF, and Hang ZH. Zak Phase Induced Multiband Waveguide by Two-Dimensional Photonic Crystals. *Opt Lett* (2017) 42:3085–8. doi:10.1364/OL.42.003085
16. Zhao W, Xu YF, Yang Y, Tao Z, and Hang ZH. Multiband Acoustic Waveguides Constructed by Two-Dimensional Phononic Crystals. *Appl Phys Express* (2020) 13:094001. doi:10.35848/1882-0786/abafc7
17. Ma T, and Shvets G. All-Si valley-hall Photonic Topological Insulator. *New J Phys* (2016) 18:025012. doi:10.1088/1367-2630/18/2/025012
18. Dong J-W, Chen X-D, Zhu H, Wang Y, and Zhang X. Valley Photonic Crystals for Control of Spin and Topology. *Nat Mater* (2017) 16:298–302. doi:10.1038/NMAT4807
19. Yan M, Lu J, Li F, Deng W, Huang X, Ma J, et al. On-chip valley Topological Materials for Elastic Wave Manipulation. *Nat Mater* (2018) 17:993–8. doi:10.1038/s41563-018-0191-5
20. Ye L, Yang Y, Hong Hang Z, Qiu C, and Liu Z. Observation of valley-selective Microwave Transport in Photonic Crystals. *Appl Phys Lett* (2017) 111:251107. doi:10.1063/1.5009597
21. Gao F, Xue H, Yang Z, Lai K, Yu Y, Lin X, et al. Topologically Protected Refraction of Robust Kink States in valley Photonic Crystals. *Nat Phys* (2018) 14:140–4. doi:10.1038/NPHYS4304
22. Shalaev MI, Walasik W, Tsukernik A, Xu Y, and Litchinitser NM. Robust Topologically Protected Transport in Photonic Crystals at Telecommunication Wavelengths. *Nat Nanotech* (2019) 14:31–4. doi:10.1038/s41565-018-0297-6
23. He X-T, Liang E-T, Yuan J-J, Qiu H-Y, Chen X-D, Zhao F-L, et al. A Silicon-On-Insulator Slab for Topological valley Transport. *Nat Commun* (2019) 10:872. doi:10.1038/s41467-019-08881-z
24. Mittal S, Fan J, Faez S, Migdall A, Taylor JM, and Hafezi M. Topologically Robust Transport of Photons in a Synthetic Gauge Field. *Phys Rev Lett* (2014) 113:087403. doi:10.1103/PhysRevLett.113.087403
25. Yang Y, Jiang H, and Hang ZH. Topological Valley Transport in Two-Dimensional Honeycomb Photonic Crystals. *Sci Rep* (2018) 8:1588. doi:10.1038/s41598-018-20001-3
26. Smirnova D, Leykam D, Chong Y, and Kivshar Y. Nonlinear Topological Photonics. *Appl Phys Rev* (2020) 7:021306. doi:10.1063/1.5142397
27. St-Jean P, Goblot V, Galopin E, Lemaître A, Ozawa T, Le Gratiet L, et al. Lasing in Topological Edge States of a One-Dimensional Lattice. *Nat Photon* (2017) 11:651–6. doi:10.1038/s41566-017-0006-2
28. Parto M, Wittek S, Hodaei H, Harari G, Bandres MA, Ren J, et al. Edge-mode Lasing in 1D Topological Active Arrays. *Phys Rev Lett* (2018) 120:113901. doi:10.1103/PhysRevLett.120.113901
29. Bahari B, Ndao A, Vallini F, El Amili A, Fainman Y, and Kanté B. Nonreciprocal Lasing in Topological Cavities of Arbitrary Geometries. *Science* (2017) 358:636–40. doi:10.1126/science.aao4551
30. Zhao H, Miao P, Teimourpour MH, Malzard S, El-Ganainy R, Schomerus H, et al. Topological Hybrid Silicon Microlasers. *Nat Commun* (2018) 9:981. doi:10.1038/s41467-018-03434-2
31. Bandres MA, Wittek S, Harari G, Parto M, Ren J, Segev M, et al. Topological Insulator Laser: Experiments. *Science* (2018) 359:eaar4005. doi:10.1126/science.aar4005
32. Zeng Y, Chattopadhyay U, Zhu B, Qiang B, Li J, Jin Y, et al. Electrically Pumped Topological Laser with valley Edge Modes. *Nature* (2020) 578:246–50. doi:10.1038/s41586-020-1981-x
33. Shao Z-K, Chen H-Z, Wang S, Mao X-R, Yang Z-Q, Wang S-L, et al. A High-Performance Topological Bulk Laser Based on Band-Inversion-Induced Reflection. *Nat Nanotechnol* (2020) 15:67–72. doi:10.1038/s41565-019-0584-x
34. *Comsol Multiphysics, v5.4* (https://cn.comsol.com)
35. Yang Y, Jia Z, Wu Y, Xiao R-C, Hang ZH, Jiang H, et al. Gapped Topological Kink States and Topological Corner States in Honeycomb Lattice. *Sci Bull* (2020) 65:531–7. doi:10.1016/j.scib.2020.01.024
36. Wu L-H, and Hu X. Scheme for Achieving a Topological Photonic crystal by Using Dielectric Material. *Phys Rev Lett* (2015) 114:223901. doi:10.1103/PhysRevLett.114.223901
37. Yang Y, Xu YF, Xu T, Wang H-X, Jiang J-H, Hu X, et al. Visualization of a Unidirectional Electromagnetic Waveguide Using Topological Photonic Crystals Made of Dielectric Materials. *Phys Rev Lett* (2018) 120:217401. doi:10.1103/PhysRevLett.120.217401

Conflict of Interest: The authors declare that the research was conducted in the absence of any commercial or financial relationships that could be construed as a potential conflict of interest.